Optimized expression and purification of NavAb provide the structural insight into the voltage dependence

Katsumasa Irie[1,2], Yukari Haga[2], Takushi Shimomura[1§], and Yoshinori Fujiyoshi[1,3].

[1]Cellular and Structural Physiology Institute (CeSPI), and [2]Graduate School of Pharmaceutical Sciences, Nagoya University, Furo-cho, Chikusa, Nagoya 464-8601, Japan.

[3]CeSPIA Inc., 2-1-1, Otemachi, Chiyoda, Tokyo, 100-0004, Japan

Address correspondence to: Katsumasa Irie, Cellular and Structural Physiology Institute (CeSPI), Nagoya University, Furo-cho, Chikusa, Nagoya 464-8601, Japan Tel.:+81-52-747-6838; Fax: +81-52-747-6795; E-mail: kirie@cespi.nagoya-u.ac.jp

[§]Present address: Division of Biophysics and Neurobiology, Department of Molecular & Cellular Physiology, National Institute for Physiological Sciences, Okazaki, Aichi, 444-8585, Japan

Running title: Structural insight of the voltage dependence of NavAb

Abstract (120 words)

Voltage-gated sodium channels are crucial for electro-signalling in living systems. Analysis of the molecular mechanism requires both fine electrophysiological evaluation and high-resolution channel structures.

Here we optimized a dual expression system of NavAb, which is a well-established standard of prokaryotic voltage-gated sodium channels, for *E.coli* and insect cells using a single plasmid vector to analyze high-resolution protein structures and measure large ionic currents.

Using this expression system, we evaluated the voltage dependence and determined the crystal structures of NavAb wild type and two mutants, E32Q and N49K, whose voltage dependences were positively shifted and essential interactions were lost in voltage sensor domain. The structural and functional comparison elucidated the molecular mechanisms of the voltage dependence of prokaryotic voltage-gated sodium channels.

Keywords

Voltage-gated sodium channel

Structural physiology

Protein expression

Abbreviations

BacNav: Prokaryotic voltage-gated sodium channel

CHAPSO: 3-[(3-Cholamidopropyl)dimethylammonio]-2-hydroxypropanesulfonate

DDM: n-Dodecyl-β-D-maltoside

DMPC: 1,2-Dimyristoyl-sn-glycero-3-phosphorylcholine

LMNG: Lauryl maltose neopentyl glycol

Nav: Voltage-gated sodium channel

Introduction

Voltage-gated sodium channels (Navs) evoke action potentials and are involved in many important physiological processes, such as neural transduction, muscle contraction, and pain sensation [1]. The propagation of action potentials is achieved mainly by selective permeation of sodium ions across cell membranes through Navs. Therefore, Navs are important targets for various therapeutics [2-4]. In eukaryotic Navs, the channel is formed by the α-subunit, which comprises four repeats of six transmembrane segments, with each repeat consisting of 300 to 400 amino acids. The α-subunit carries several glycosylation sites and co-assembles with auxiliary subunits to form the native channel [5]. Structures of eukaryotic Navs are obtained by cryo-electron microscopic (cryoEM) single particle analysis [6, 7]. These structures provide information about the whole structure, such as the domain arrangement, and allow for prediction of the drug binding site or residues involved in genetic diseases. The limited resolution, however, makes it is difficult to reveal the underlying molecular mechanisms.

Prokaryotic Navs (BacNavs) are rather simple tetrameric cation channels, comprising monomers of fewer than 300 amino acids [8-11]. Their structural simplicity makes BacNavs useful for analyzing the basic molecular mechanisms of Navs. Structures of various homologues of BacNavs in different states were solved by X-ray crystallography [12-17] or electron microscopy [18], and functional studies [19, 20] of wild-type (WT) and mutant BacNavs have provided insight into the molecular mechanisms of Navs. NavAb was cloned from *Arcobacter butzleri* and the structure was solved as the first full-length structure of Nav at atomic resolution by X-ray crystallography [12]. NavAb provided the first insight into the characteristic features of Navs, such as the additional helix (P2-helix) in the extracellular vestibule of the channel pore and the lateral fenestrations in the lipid-bilayer sides of the pore domain. These features helped to clarify the eukaryotic channel structure based on cryo-EM single particle analysis. However, several important issues of sodium channels, such as the molecular bases of the sodium-ion selectivity, the voltage dependence and the inhibitor binding, have not been completely clarified although the comprehensive studies provided interesting insight [16, 20, 21].

Understanding how mutations of particular residues alter the functional activity of BacNav will help to elucidate the molecular mechanisms. In a previous study [12], NavAb protein was obtained from an insect cell baculovirus expression system, which provides high-yield protein expression but virus amplification requires several weeks for large-scale expression. This is a rate-limiting step of structure-function studies based on mutational analysis. Furthermore, baculoviruses are lysogenically released from the plasma membrane of the host cell after transfection [22], which interferes with electrophysiological measurement. To improve the structural and functional analysis systems of NavAb, we constructed a dual expression system of NavAb in *E.coli* and insect cells, and determined three crystal structures of NavAb wild type and

two mutants. These results provided the structural insight of voltage dependence of NavAb.

Materials and Methods

Protein expression and purification

The NavAb DNA was synthesised by Genscript Inc. and subcloned into modified pBiEX-1 vector (Novagen) that was modified by replacing the fragment from NcoI site (CCATGG) to SalI site (GTCGAC) in multi cloning site with the sequence "CCATGGGCAGCAGCCATCATCATCATCATCACAGCAGCGGCCTGGTGCCGCGCGGCAGCCATATGCTCGAGCTGGTGCCGCGCGGCAGCGGATCCTAAGTCGAC" to add the N-terminal His tag and thrombin cleavage site. The NavAb DNA was subcloned between BamHI site (GGATCC) and SalI site. Proteins were expressed in the *E. coli* KRX strain (Promega). Cells were grown at 37ºC to an OD_{600} of 0.8, induced with 0.1% rhamnose (Wako), and grown for 16 h at 18ºC. The cells were suspended in TBS buffer (20 mM Tris-HCl pH 8.0, 150 mM NaCl) and lysed using a French Press (SLM AMINCO) at 12,000 psi. Cell debris was removed by low-speed centrifugation (12,000×g, 30 min, 4°C). Membranes were collected by centrifugation (100,000×g, 1 h, 4°C) and solubilized by homogenization in TBS buffer containing 1.5 % n-dodecyl-β-D-maltoside (DDM, Anatrace). After centrifugation (40,000×g, 30 min, 4°C), the supernatant was loaded onto a HIS-Select® Cobalt Affinity Gel column (Sigma). The column was washed with 10 mM imidazole in TBS buffer containing 0.05 % DDM, and the protein was eluted with 300 mM imidazole. Eluted protein was purified on a Superdex-200 column (GE Healthcare) in TBS buffer containing 0.05 % DDM.

Thermostability assay of purified proteins

The purified proteins were subjected to a tryptophan fluorescence-detection size-exclusion chromatography-based thermostability assay [23]. The 300-ng purified proteins in 50-µl TBS buffer containing 0.05 % DDM or 0.05% lauryl maltose neopentyl glycol (LMNG, Anatrace) were incubated at 4˚C to 90˚C for 10 min, using a thermal cycler, and then centrifuged at 40,000 × g for 30 min. The supernatant (50 µl) was loaded onto a Superdex 200 Increase 5/150 GL column (GE Healthcare). The eluate from the SEC column was passed through a fluorometer (280 nm excitation and 340 nm emission). The peak heights were normalized to that of samples incubated at 4˚C, and melting temperatures (T_m) were determined by fitting the curves to a sigmoidal dose-response equation.

Protein purification for crystallization

The protein bound to the cobalt affinity column was washed with 10 mM imidazole in TBS buffer containing 0.05% LMNG instead of DDM. After washing, the protein was eluted with 300

mM imidazole and, purified on a Superdex-200 column in TBS buffer containing 0.05% LMNG.

Crystallization and structural determination

Before crystallization, the purified protein was concentrated to ~20mg ml^{-1} and reconstituted into a bicelle solution [24], containing a 10% bicelle mixture at 2.8:1 (1,2-dimyristoyl-sn-glycero-3-phosphorylcholine [DMPC, Anatrace]: 3-[(3-cholamidopropyl)dimethylammonio]-2-hydroxypropanesulfonate [CHAPSO, DOJINDO]). The NavAb-bicelle preparation was mixed in a 10:1 ratio. Crystals were grown by sitting-drop vapor diffusion at 20°C by mixing 300-nl volumes of the protein solution (8–18 mg/ml) and the reservoir solution (9%–11% polyethylene glycol [PEG] monomethyl ether 2000, 100 mM NaCl, 100 mM calcium nitrate, and 100 mM Tris-HCl, pH 8.4) with mosquito LCP (TTP Labtech). All crystals were cryoprotected by 25 % (v/v) DMSO and flash frozen in liquid nitrogen.

All data were collected at BL41XU and BL32XU of SPring-8 and processed using HKL2000. Analyses of the data with the University of California Los Angeles anisotropy server [25] revealed that WT crystals were severely anisotropic with an effective resolution of 2.8 Å in the c^* direction, but only 3.4 Å in the a^* and b^* directions. The data were ellipsoidally truncated and rescaled to minimize the inclusion of poor diffraction data.

The initial phase was obtained using a molecular replacement method with PHASER[26]. The final model was constructed in COOT [27] and refined at 2.8Å in refmac5 [28] and Phenix [29]. Data collection and refinement statistics of all crystals are summarized in Table 1.

Transient protein expression in insect cells

SF-9 cells were grown in Sf-900™ III medium (Gibco) complemented with 0.5% 100× Antibiotic-Antimycotic (Gibco) at 27°C. Cells were transfected with NavAb-cloned pBiEX vectors and enhanced green fluorescent protein (EGFP)-cloned pBiEX vectors using Fugene HD transfection reagent (Promega). The NavAb-cloned vector (2 μg) was mixed with 0.5μg of the EGFP-cloned vector in 3-μL Fugene HD reagent. Next, 100μL of the culture medium was added and the mixture was incubated for 10 min before the transfection mixture was gently dropped on 3 mL cultured medium containing 0.6×10^6 cells. After incubation for 24-48 h, the cells were used for the electrophysiological measurements.

Electrophysiological measurement of insect cells

Cells were voltage-clamped with an EPC10 amplifier (HEKA Elektronik, Lambrecht, Germany). The pipette solution contained 105 mM CsF, 35 mM NaCl, 10 mM EGTA, and 10 mM HEPES (pH 7.4). The bath solution contained 150 mM NaCl, 1.5 mM $CaCl_2$, 1 mM $MgCl_2$, 2 mM KCl, 10 mM HEPES (pH 7.4), and 10 mM glucose. Patch pipette resistances were 2–3.5

MΩ. Data were collected with the Patchmaster program (HEKA). To measure the inactivation by repetitive pulses at a negative holding potential, the bath solution was replaced by the measurement solution (150 mM NaCl, 5 mM $CaCl_2$, 1 mM $MgCl_2$, 2 mM KCl, 10 mM HEPES (pH 7.4), and 10 mM glucose). The bath solutions were changed using the Dynaflow® Resolve system. All experiments were conducted at 25°C ± 2°C. All results are presented as mean ± standard error.

Results and Discussion

Crystallization of NavAb obtained from the *E.coli* expression system

NavAb DNA was cloned into a pBiEX-1 vector, which is a dual expression vector for both *E.coli* and insect cell systems, and transformed to the *E.coli* system of KRX strain, which has high transformation efficiency and produces large amounts of protein. By single-step transformation of sub-cloning or mutagenesis, we are able to obtain both an *E.coli* host for large-scale protein expression and sufficient amounts of the plasmid for insect cell transient expression.

The NavAb protein was solubilized by DDM (Fig. S1a) and well purified through metal-chelate affinity chromatography and gel filtration chromatography as a 25.9-kDa protein (Fig. 1a). From 1 liter of the culture medium, 2mg proteins were obtained. The thermal stability of the purified protein was evaluated using the tryptophan fluorescence-detection size-exclusion chromatography-based thermostability assay method [23]. The T_m value (temperature at which half of the protein was aggregated) was 54.6°C (Fig. 1b), which seemed adequate for crystallization, but the DDM-purified protein was not crystallized on sitting-drop vapor diffusion with or without the bicelle mixture. To retain the purified protein in more intact condition, DDM was exchanged with a lipid-like detergent LMNG (Fig. S1b) after solubilization. After binding to the metal-chelate affinity resin, the protein was eluted and further purified by gel filtration chromatography under LMNG conditions. The amount of purified protein per liter of the culture medium was decreased to less than 1 mg, but T_m value was improved to 64.0°C (Fig. 1b).

Protein purified with LMNG was used for crystallization with the bicelle method. Using a similar ratio of protein per bicelle as in previous reports [12, 30], small crystals were obtained under PEG400 conditions after 2 months incubation (Fig. 2a). Without bicelle, thin platelet crystals appeared under the same condition (Fig. 2b). On the other hand, under conditions in which the bicelle content was decreased to one-twentieth that of the protein (w/w), pyramidal crystals were obtained under PEG monomethyl ether 2000 and pH 8.4 conditions after incubation for several days (Fig. 2c). In the condition containing less of the bicelle mixture, the two alkyl chains of LMNG may behave like a lipid to stabilize the channel structure on behalf of

DMPC (Fig. S1c).The pH value and ionic concentration of the crystallization condition were different from those reported previously (pH 4.75 and approximately 2M ammonium sulphate) [12, 30], and similar to those of sea water [31]. The crystals of our purified protein tended to be smaller and more rectangle in lower-pH condition. The low limit of crystallization pH was 6.0 of cacodylate-NaOH buffer (Fig. 2d), but whose crystals provided poor diffraction spots.

Crystal structure of the NavAb WT in the high-pH condition.

The resolution of the diffraction data obtained from a single crystal growing in pH 8.4 condition reached 2.8 Å. The cell parameters (*a*=126.5 Å, *b*=126.5 Å, *c*=201.7 Å) were similar to those in a previous report [12, 30]. The crystal structure of NavAb WT in our high-pH condition, called high-pH NavAb WT, was determined by molecular replacement using NavAb I217C monomer (pdb code: 3RVY) as the initial model and finally improved to a 2.8Å-resolution structure with some detergents and lipids (Fig. 2e-g). The space group of crystal was *I*422 and the asymmetric unit in the crystal lattice contained one monomer. The tetrameric channel was formed by four-fold symmetry of the *c*-axis. The root mean square deviation (RMSD) between monomers of high-pH NavAb WT to each A and B chain of NavAb I217C was 0.57Å and 0.56Å, respectively. The crystallographic interaction of high-pH NavAb WT was similar at a glance, but substantially different from that of NavAb I217C (Fig. S2a-d). One channel of the high-pH NavAb WT was rotated approximately 17° clockwise on the *c*-axis from the extracellular side view, and the adjacent channel interacting with the VSD was also rotated in the counter clockwise direction (Fig. S2e).

In the lateral fenestration, which is located between the transmembrane parts of the two pore subunits, a long and thin electron density was observed and connected to the large density in the hydrophilic inner vestibule. This electron density corresponded to the alkyl chain and the maltoside of DDM in the lateral fenestration and inner vestibule, respectively (Fig. 2f). The similar density was observed in NavAb I217C structure [12]. Strong electron density, which was well fitted to the hydrophobic part of CHAPSO (Fig. S2d), was observed between the cytoplasmic end of the pore-domain S5 helix and the adjacent-subunit voltage sensor domain (VSD) (Fig. 2g). Four VSDs are individually located around the channel pore and connected to the pore domain by a S4-S5 linker helix. Therefore, it is thought that CHAPSO observed between the pore domain and the S4-S5 linker acts as a critical wedge to closely tether the VSDs to the tetrameric channel pore in solubilized condition. CHAPSO was also observed in the closed structure of NavAb mutant (pdb code: 5VB2) [17], but the positions of CHAPSO in each structure were different (Fig. S3). In the closed structure of NavAb mutant, two molecules of CHAPSO bound the C-terminus of S6 helix of pore domain, which plays the activation gate in the channel opening. The conformation of the mutant was stabilized to the closed conformation by mutations. The differences of the CHAPSO

position would come from the differences of the conformations and the crystallization conditions of each structure.

Previously, the NavAb WT structure was determined in low-pH and high-ionic conditions (pdb code: 4EKW) [30] and represented the dimer-of-dimer rectangle channel (Fig. 3a), with a asymmetric selectivity filter (Fig. 3b), which differed from that of high-pH NavAb WT. The full-length structure of other BacNavs homologues also showed the square shape channel structure [14, 18]. The crystallization condition of high-pH NavAb WT is similar to the living condition of the host bacterium of NavAb. Therefore, it is plausible that the structure of high-pH NavAb WT could represent one of the native conformations. On the other hand, it is difficult to determine why the low-pH NavAb WT structure was asymmetric. Considering the shapes of crystal tend to reflect the protein symmetry in the crystal, the small rectangle crystals obtained in low-pH condition (Fig. 2d) suggested the possibility that the low pH is the main factor of the distorted channel structure, although it could not completely exclude the other factor.

Electrophysiological studies of NavAb with the insect cell transient expression system.

NavAb WT originally exhibited irreversible inactivation in a use-dependent manner [12]. Therefore, the structure of the low-pH NavAb WT was assigned as the inactivated conformation called the “late-slow inactivation” form [30]. By transient expression in insect cells, NavAb WT showed run-down currents at a holding potential of -180mV (Fig. 4a, c), but it is possible that NavAb requires a much more negative holding potential to recover from the inactivation. Maintaining the membrane potential at a more negative voltage than -180 mV for a long time, however, was very difficult. Alternatively, a short pulse (100 ms) of -240 mV was given to the cell membrane before the depolarization stimulus. In this protocol, run-down of the current of NavAb WT was not observed (Fig. 4b, c). These results indicated that measurement of NavAb WT at a -240-mV holding potential could show stable currents. The membrane potentials of some bacteria are very negative [32]. The resting membrane potential of the host bacterium of NavAb (*Arcobacter butzleri*) might be more negative than -180mV. Therefore, it is suggested that NavAb is tuned to work at a more negative membrane resting potential, and that the “late slow inactivation” is due to the accumulation of voltage-dependent inactivation under an insufficient holding potential.

The use-dependent inactivation of NavAb WT was closely related to the voltage dependence of the steady-state inactivation. E43K and D60K of NaChBac, a BacNav homologue of *Bacillus halodurans*, are well known mutations that positively shift the voltage dependence of the activation [33]. Glu43 and Asp60 of NaChBac correspond to Glu32 and Asn49 of NavAb. E32Q and E32K mutations were introduced to NavAb. NavAb E32K did not show any measurable current. On the other hand, NavAb E32Q displayed an inward current that was decreased by

repetitive depolarization pulses at a holding potential of -140mV (Fig. 4d, f). This characteristic was similar to the use-dependent inactivation of NavAb WT at the -180 mV holding potential. The current of NavAb E32Q was not reduced at a -140mV holding potential with a short interval pulse of -180 mV (Fig. 4e, f). These results suggested that the E32Q mutation positively shifted the voltage dependence of the steady-state inactivation. The N49K mutation of NavAb also does not exhibit use-dependent inactivation, and positively shifts the voltage dependence [34]. In the transient expression system, the NavAb N49K currents were also stably measured and did not display use-dependent inactivation even at a holding potential of -140 mV (Fig. 4g, h). These results suggested that NavAb E32Q is an intermediate between the WT and N49K mutant.

Crystal structure of the NavAb mutants.

To reveal how the single mutations, E32Q and N49K, changed the voltage dependence, the structures of the E32Q and N49K mutants were solved by the same method as the high-pH NavAb WT. The structures of E32Q and N49K were determined at a resolution of 3.4 Å. Their overall structures were similar to that of the WT. The RMSDs of each E32Q or N49K mutant to the WT were 0.45 or 0.55 Å, respectively. The pore domain of each mutant was almost the same as that of the WT (RMSDs were below 0.32 Å). Superimposing each mutant to WT NavAb on the pore domain to clarify differences in the VSDs revealed slight deviations in the S3-S4 loop of the E32Q mutant and in the S2-S3 helices of the N49K mutant compared with the WT structure (Fig. 5a and b). The location of the S2 and S3 helices of the N49K mutant was approximately 1 Å farther from the pore domain than those of the WT (Fig. 5b). Mutated residues, Glu32 and Asn49, were located in the S1 and S2 helices, respectively. These residues play an important role by interacting with arginine residues of the S4 helix (Arg99, Arg102 and Arg105; Fig. 5c). At the depolarization, these arginine residues move toward the extracellular side. It is thought that Glu32 and Asn49 sequentially interact with the arginine residues to lift up the S4 helix, which leads to channel activation [33]. In NavAb WT, Asn49 forms a hydrogen bond with Arg105 (3.2Å), and Glu32 is close enough to form a weak salt bridge to Arg99 (4.2Å) (Fig. 5c: left). In NavAb E32Q, an Asn49-Arg105 interaction was observed, but Gln32, which was farther from Arg99 than in the WT, exhibited no interactions with any other arginine residues (Fig. 5c: middle). In the N49K mutant, Lys49 formed a tight salt bridge with Glu32, in which no arginine residues interacted with Glu32 and Lys49 (Fig. 5c: right). This newly formed interaction seems to render the S1 and S2 helices distant from the S4 helix. Due to the loss of these interactions, each mutant is thought to require a larger depolarization for activation.

Vertical orientation of the VSD.

To evaluate the relationship between the voltage dependence and the VSD structure, we

compared the high-pH NavAb structure to that of NavMs as a functional BacNav homologue whose structure was also solved with the VSD [14]. NavMs showed stable currents at a holding potential of -180mV. Considering that recovery of NavAb is postulated to occur at -240 mV, the voltage dependence of NavMs should be more positive than that of NavAb. Each pore domain (S5-S6 helices) and VSD (S1-S4 helices) of NavMs was well superimposed on that of NavAb (RMSD =0.62Å and 1.33Å, respectively) (Fig. 6a and b). When superimposed with the pore domain, however, the S4-S5 linker helix of NavMs was located more on the cytosolic side than that of NavAb (Fig. 6c). The VSD of both NavAb and NavMs was thought to be the activated conformation, because there was no electrical potential between the cytosolic and extracellular sides of these structures in the crystal packing. The vertical position of the S4-S5 linker helix in the activated state might affect the voltage dependence.

Our dual expression system allowed us to elucidate the molecular mechanisms of voltage dependence by comparing the structure and function of WT and two mutant voltage-gated sodium channels. The molecular mechanism of the ion selectivity of sodium channel is also important to be revealed. Analysis of the ion selectivity requires both fine electrophysiological evaluation of the reversal potential in various ionic conditions and a high-resolution protein structure. This dual expression system allows for facile and rapid evaluation and comparison of the function and structure of prokaryotic cation channels, and will therefore facilitate elucidation of the detailed mechanisms of sodium ion selectivity.

Acknowledgements

The synchrotron radiation experiments were performed at BL41XU and BL32XU in SPring-8 with the approval of the Japan Synchrotron Radiation Research Institute (JASRI) (Proposal number 2011B1240, 2012B1066, 2012B1966, 2013A1112, 2013B1178, 2014A1248, 2014B1165, 2015A1090, 2015B1042 and 2016B2721) and the Platform Project for Supporting Drug Discovery and Life Science Research. We thank the beamline staff for their excellent facilities and support. This work was supported by Grants-in-Aid for Scientific Research (S), Grant-in-Aid for Young Scientists (B), the Japan Agency for Medical Research and Development and Toyoaki Scholarship Foundation.

References

1. Hille B (2001) *Ion Channels of Excitable Membranes*, 3rd ed. Sinauer. Sunderland, MA.
2. Dib Hajj SD, Cummins TR, Black JA & Waxman SG (2010) Sodium channels in normal

and pathological pain. *Annu. Rev. Neurosci.* **33,** 325-347.

3. Waxman SG, Cummins TR, Black JA & Dib Hajj S (2002) Diverse functions and dynamic expression of neuronal sodium channels. *Novartis. Found. Symp.* **241,** 34-51.
4. Waxman SG, Dib Hajj S, Cummins TR & Black JA (2000) Sodium channels and their genes: dynamic expression in the normal nervous system, dysregulation in disease states(1). *Brain Res.* **886,** 5-14.
5. Catterall WA (2000) From ionic currents to molecular mechanisms: the structure and function of voltage-gated sodium channels. *Neuron* **26,** 13-25.
6. Shen H, Zhou Q, Pan X, Li Z, Wu J & Yan N (2017) Structure of a eukaryotic voltage-gated sodium channel at near-atomic resolution. *Science* **355**, doi: 10.1126/science.aal4326.
7. Yan Z, Zhou Q, Wang L, Wu J, Zhao Y, Huang G, Peng W, Shen H, Lei J & Yan N (2017) Structure of the Nav1.4-beta1 complex from electric eel. *Cell.* **170,** 470-482.e11 .
8. Ren D, Navarro B, Xu H, Yue L, Shi Q & Clapham DE (2001) A prokaryotic voltage-gated sodium channel. *Science* **294,** 2372-2375.
9. Koishi R, Xu H, Ren D, Navarro B, Spiller BW, Shi Q & Clapham DE (2004) A superfamily of voltage-gated sodium channels in bacteria. *J. Biol. Chem.* **279,** 9532-9538.
10. Ito M, Xu H, Guffanti AA, Wei Y, Zvi L, Clapham DE & Krulwich TA (2004) The voltage-gated Na^+ channel NaVBP has a role in motility, chemotaxis, and pH homeostasis of an alkaliphilic Bacillus. *Proc. Natl. Acad. Sci. U. S. A.* **101,** 10566-10571.
11. Irie K, Kitagawa K, Nagura H, Imai T, Shimomura T & Fujiyoshi Y (2010) Comparative study of the gating motif and C-type inactivation in prokaryotic voltage-gated sodium channels. *J. Biol. Chem.* **285,** 3685-3694.
12. Payandeh J, Scheuer T, Zheng N & Catterall WA (2011) The crystal structure of a voltage-gated sodium channel. *Nature* **475,** 353-358.
13. Irie K, Shimomura T & Fujiyoshi Y (2012) The C-terminal helical bundle of the tetrameric prokaryotic sodium channel accelerates the inactivation rate. *Nat. Commun.* **3,** 793.
14. Sula A, Booker J, Ng LC, Naylor CE, DeCaen PG & Wallace BA (2017) The complete structure of an activated open sodium channel. *Nat. Commun.* **8,** 14205.
15. Shaya D, Findeisen F, Abderemane Ali F, Arrigoni C, Wong S, Nurva SR, Loussouarn G & Minor DL Jr (2014) Structure of a prokaryotic sodium channel pore reveals essential gating elements and an outer ion binding site common to eukaryotic channels. *J. Mol. Biol.* **426,** 467-483.
16. Naylor CE, Bagnéris C, DeCaen PG, Sula A, Scaglione A, Clapham DE & Wallace BA (2016) Molecular basis of ion permeability in a voltage-gated sodium channel. *EMBO. J.* **35,** 820-830.

17. Lenaeus MJ, Gamal El Din TM, Ing C, Ramanadane K, Pomes R, Zheng N & Catterall WA (2017) Structures of closed and open states of a voltage-gated sodium channel. *Proc. Natl. Acad. Sci. U. S. A.* **114,** E3051-E3060.
18. Tsai CJ, Tani K, Irie K, Hiroaki Y, Shimomura T, McMillan DG, Cook GM, Schertler GF, Fujiyoshi Y & Li XD (2013) Two alternative conformations of a voltage-gated sodium channel. *J. Mol. Biol.* **425,** 4074-408.
19. Lee S, Goodchild SJ & Ahern CA (2012) Local anesthetic inhibition of a bacterial sodium channel. *J. Gen. Physiol.* **139,** 507-516.
20. Shimomura T, Irie K & Fujiyoshi Y (2016) Molecular determinants of prokaryotic voltage-gated sodium channels for recognition of local anesthetics. *FEBS J.* **283,** 2881-2895.
21. Ulmschneider MB, Bagnéris C, McCusker EC, Decaen PG, Delling M, Clapham DE, Ulmschneider JP & Wallace BA (2013) Molecular dynamics of ion transport through the open conformation of a bacterial voltage-gated sodium channel. *Proc. Natl. Acad. Sci. U. S. A.* **110,** 6364-6369.
22. Kost TA, Condreay JP & Jarvis DL (2005) Baculovirus as versatile vectors for protein expression in insect and mammalian cells. *Nat. Biotechnol.* **23,** 567-575.
23. Hattori M, Hibbs RE & Gouaux E (2012) A fluorescence-detection size-exclusion chromatography-based thermostability assay for membrane protein precrystallization screening. *Structure* **20,** 1293-1299.
24. Faham S, Boulting GL, Massey EA, Yohannan S, Yang D & Bowie JU (2005) Crystallization of bacteriorhodopsin from bicelle formulations at room temperature. *Protein. Sci.* **14,** 836-840.
25. Strong M, Sawaya MR, Wang S, Phillips M, Cascio D & Eisenberg D (2006) Toward the structural genomics of complexes: crystal structure of a PE/PPE protein complex from Mycobacterium tuberculosis. *Proc. Natl. Acad. Sci. U. S. A.* **103,** 8060-8065.
26. McCoy AJ, Grosse Kunstleve RW, Adams PD, Winn MD, Storoni LC & Read RJ (2007) Phaser crystallographic software. *J. Appl. Crystallogr.* **40,** 658-674.
27. Emsley P, Lohkamp B, Scott WG & Cowtan K (2010) Features and development of COOT. *Acta. Crystallogr. D. Biol. Crystallogr.* **66,** 486-501.
28. Murshudov GN, Vagin AA & Dodson EJ (1997) Refinement of macromolecular structures by the maximum-likelihood method. *Acta. Crystallogr. D. Biol. Crystallogr.* **53,** 240-255.
29. Adams PD, Afonine PV, Bunkóczi G, Chen VB, Davis IW, Echols N, Headd JJ, Hung LW, Kapral GJ, Grosse-Kunstleve RW, McCoy AJ, Moriarty NW, Oeffner R, Read RJ, Richardson DC, Richardson JS, Terwilliger TC & Zwart PH. (2010) PHENIX: a comprehensive Python-based system for macromolecular structure solution. *Acta Crystallogr. D. Biol Crystallogr.* **66,** 213-221.

30. Payandeh J, Gamal El-Din TM, Scheuer T, Zheng N & Catterall WA (2012) Crystal structure of a voltage-gated sodium channel in two potentially inactivated states. *Nature* **486,** 135-139.
31. Wakita M, Watanabe S, Honda M, Nagano A, Kimoto K, Matsumoto K, Kitamura M, Sasaki K, Kawakami H, Fujiki T, Sasaoka K, Nakano Y, & Murata A (2013) Ocean acidification from 1997 to 2011 in the subarctic western North Pacific Ocean. *Biogeosciences* **10**, 7817-7827.
32. Hirota N & Imae Y (1983) Na^+-driven flagellar motors of an alkalophilic Bacillus strain YN-1. *J. Biol. Chem.* **258,** 10577-10581.
33. Shimomura T, Irie K, Nagura H, Imai T & Fujiyoshi Y. (2011) Arrangement and mobility of the voltage sensor domain in prokaryotic voltage-gated sodium channels. *J. Biol. Chem.* **286,** 7409-7417.
34. Gamal El Din TM, Martinez GQ, Payandeh J, Scheuer T & Catterall WA (2013) A gating charge interaction required for late slow inactivation of the bacterial sodium channel NavAb. *J. Gen. Physiol.* **142,** 181-190.

Table 1 Data collection and refinement statistics

	NavAb WT	E32Q	N49K
PDB entry	**5YUA**	**5YUB**	**5YUC**
Wavelength		1.00	
Resolution range	31.46 - 2.8	41.06 - 3.4	41.17 - 3.4
	(2.90 - 2.8)	(3.52 - 3.4)	(3.52 - 3.4)
Space group		*I* 4 2 2	
Unit cell	126.5 126.5 201.7	127.0 127.0 202.6	127.4 127.4 202.8
	90 90 90	90 90 90	90 90 90
Total reflections	184311 (18603)	163165 (15541)	160929 (15367)
Unique reflections	20186 (505)	11773 (259)	11809 (306)
Multiplicity	9.1 (9.3)	13.9 (13.3)	13.6 (13.4)
Completeness (%)	87.68 (25.29)	86.42 (22.21)	87.26 (26.56)
Mean I/sigma(I)	14.02 (1.05)	14.86 (1.80)	13.60 (1.65)
R_{merge}	0.248 (3.136)	0.243(1.924)	0.250 (2.307)
R_{pim}	0.087 (1.074)	0.0689 (0.543)	0.0708 (0.650)
CC1/2	0.995 (0.431)	0.998 (0.845)	0.997 (0.61)
R_{work}	0.230 (0.383)	0.240 (0.243)	0.230 (0.247)
R_{free}	0.262 (0.340)	0.273 (0.313)	0.278 (0.378)
Non-hydrogen atoms No.	2248	1931	1932
macromolecules	1860	1865	1866
ligands	379	66	66
solvent	9		
Protein residues	228	229	229
RMS(bonds)	0.010	0.011	0.011
RMS(angles)	1.13	1.16	1.15
Ramachandran favoured (%)	95.58	95.59	91.63
Ramachandran allowed (%)	4.42	4.41	8.37
Ramachandran outliers (%)	0.00	0.00	0.00
Average B-factor	88.74	61.17	51.83
macromolecules	82.38	60.05	49.68
ligands	120.70	92.73	112.56

Figure legends

Fig. 1

Purified proteins of NavAb WT and thermal stability under DDM or LMNG conditions.
a: Sodium dodecyl sulfate-polyacrylamide gel electrophoresis of purified NavAb WT protein. Left lane: protein eluted from Cobalt Affinity Gel column. Right lane: purified protein after size-exclusion chromatography.
b: Thermostability of NavAb WT in the DDM condition (closed circle) and the LMNG condition (open circle).

Fig. 2

Crystals and structure of NavAb WT in a high-pH condition
a: First crystal obtained from the initial screening in the PEG400 condition. b: Crystal growing without bicelle mixture. c: Optimized crystal. d: Crystal growing in lower pH condition (cacodylate-NaOH buffer, pH 6.0) than that of Optimized crystal. Scale bar indicates 100μm (a-d). e: Electron density map of the NavAb tetramer viewed from the cytosolic side. The carbon atoms of each subunit are colored each different color (green, cyan, magenta and gray). The carbon atoms of CHAPSO, DDM and neighboring lipid are colored yellow, orange, and pink, respectively. f: Binding site of CHAPSO. g: Electron density of DDM in the inner vestibule and viewed from the middle of lipid bilayer to the cytosolic side. The S5 and S6 helices of the channel tetramer were colored same in e.

Fig. 3

Structural comparison of NavAb WT in high- and low-pH conditions.
a: Structure of whole channels of NavAb WT in a low-pH condition (pdb code: 4EKW) superimposed on that in a high-pH condition (white). Chain A and B of low-pH NavAb WT are colored orange and blue, respectively. b: Structure of the selectivity filter of the low-pH NavAb WT superimposed on that of the high-pH NavAb. For clarity, the selectivity filters coming from two face-to-face subunits are depicted in each channel.

Fig. 4

Use-dependent inactivation of NavAb WT and mutants.
a,d and g: Representative traces of NavAb WT(a), and E32Q(d) and N49K(g) mutants without a short pre-pulse, respectively. b and e: Representative traces of NavAb WT(b) and E32Q(e) mutant with a short pre-pulse, respectively. c, f and h: Normalised current of NavAb WT(c), and E32Q(f) and N49K(h) mutants without (closed circle) or with (open circle) a short pre-pulse,

respectively.

Fig. 5

Structural comparison of NavAb and the E32Q and N49K mutants

a: Distance from the main-chain Cα carbon of NavAb WT to that of NavAb E32Q (black line) and NavAb N49K (red line) mutant in the corresponding residues. b : Structure of the pore domain of NavAb E32Q (green) or N49K (cyan) mutant superimposed on that of NavAb WT (white), respectively. c: Interaction between charged residues of the S3 helix to the arginine repeat of the S4 helix in the VSD. The observed interactions are indicated as dashed red line in c.

Fig. 6

Structural comparison of NavAb with NavMs

a and b: Structure of the pore domain and the VSD of NavMs (magenta) superimposed on that of NavAb WT (white), respectively. c: Shift to the cytosolic side of NavMs VSD and the S4-S5 linker helix in horizontal viewing of a. “Ext.” and “Cyto.” indicate extracellular and cytoplasmic side, respectively. For clarity, the S1-S3 helices of NavAb and NavMs are omitted in c. The segments coming from adjacent subunit are indicated with prime symbol.

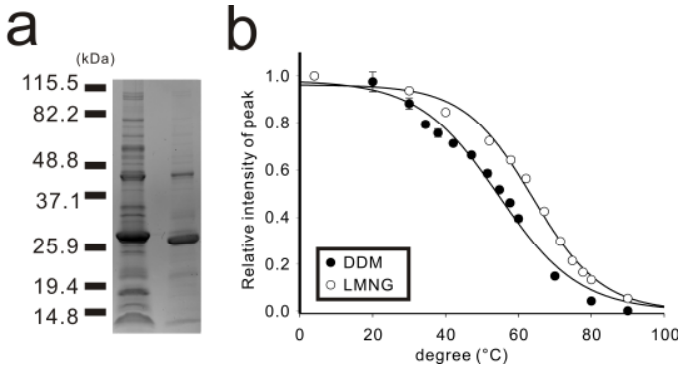
a
(kDa)
115.5
82.2
48.8
37.1
25.9
19.4
14.8
b
Relative intensity of peak
1.0
0.8
0.6
0.4
0.2
0.0
DDM
LMNG
0
20
40
60
80
100
degree (°C)

Figure.1

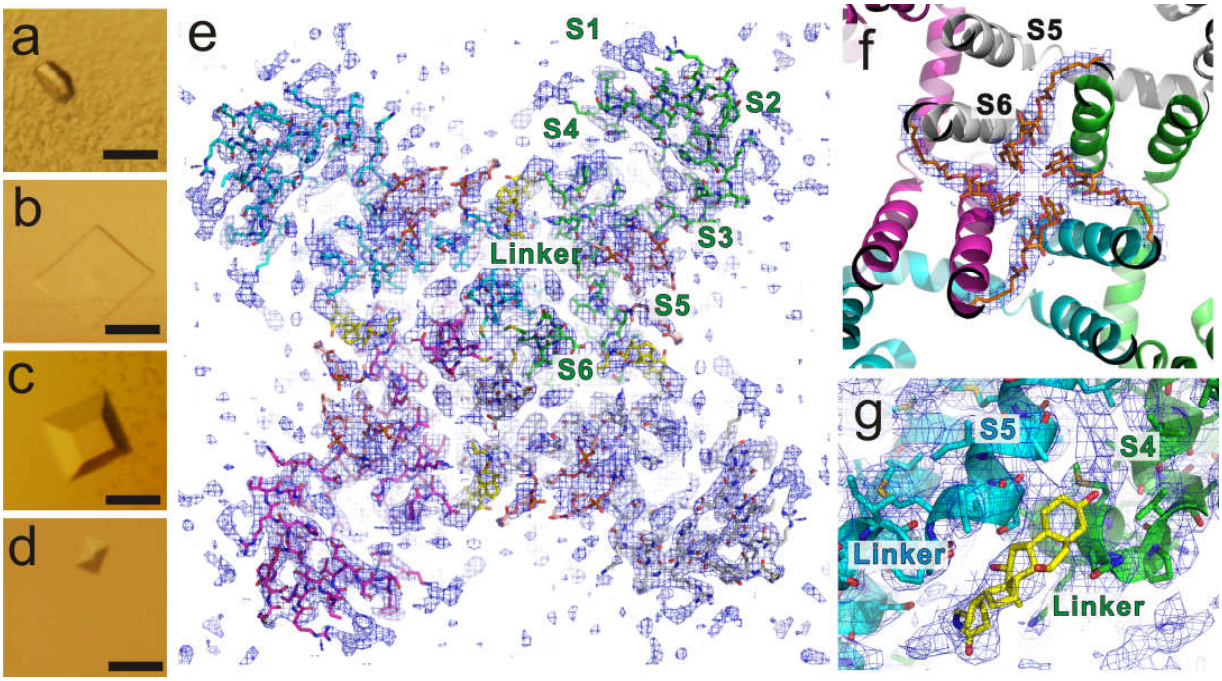

Figure.2

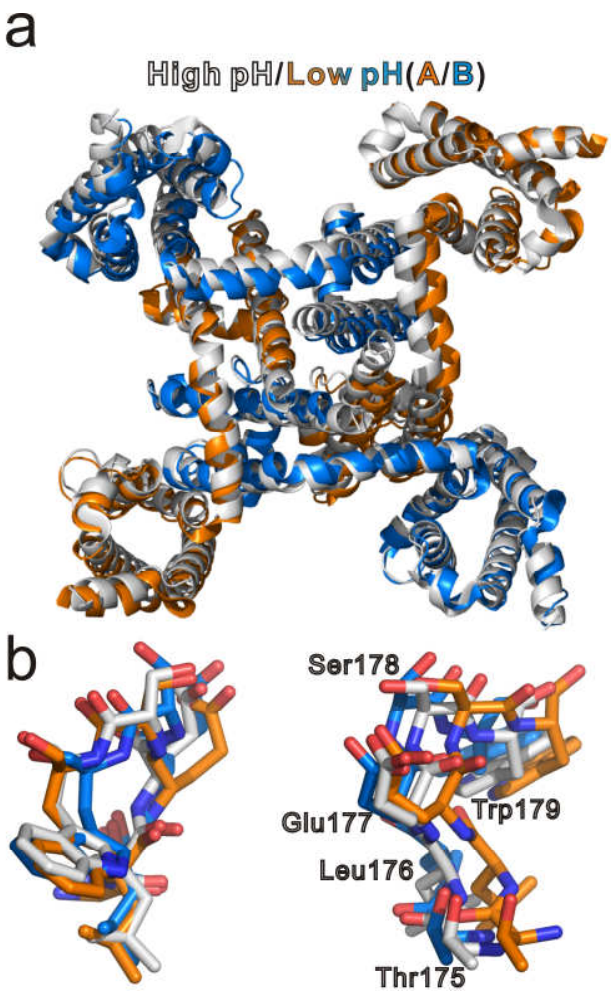

Figure.3

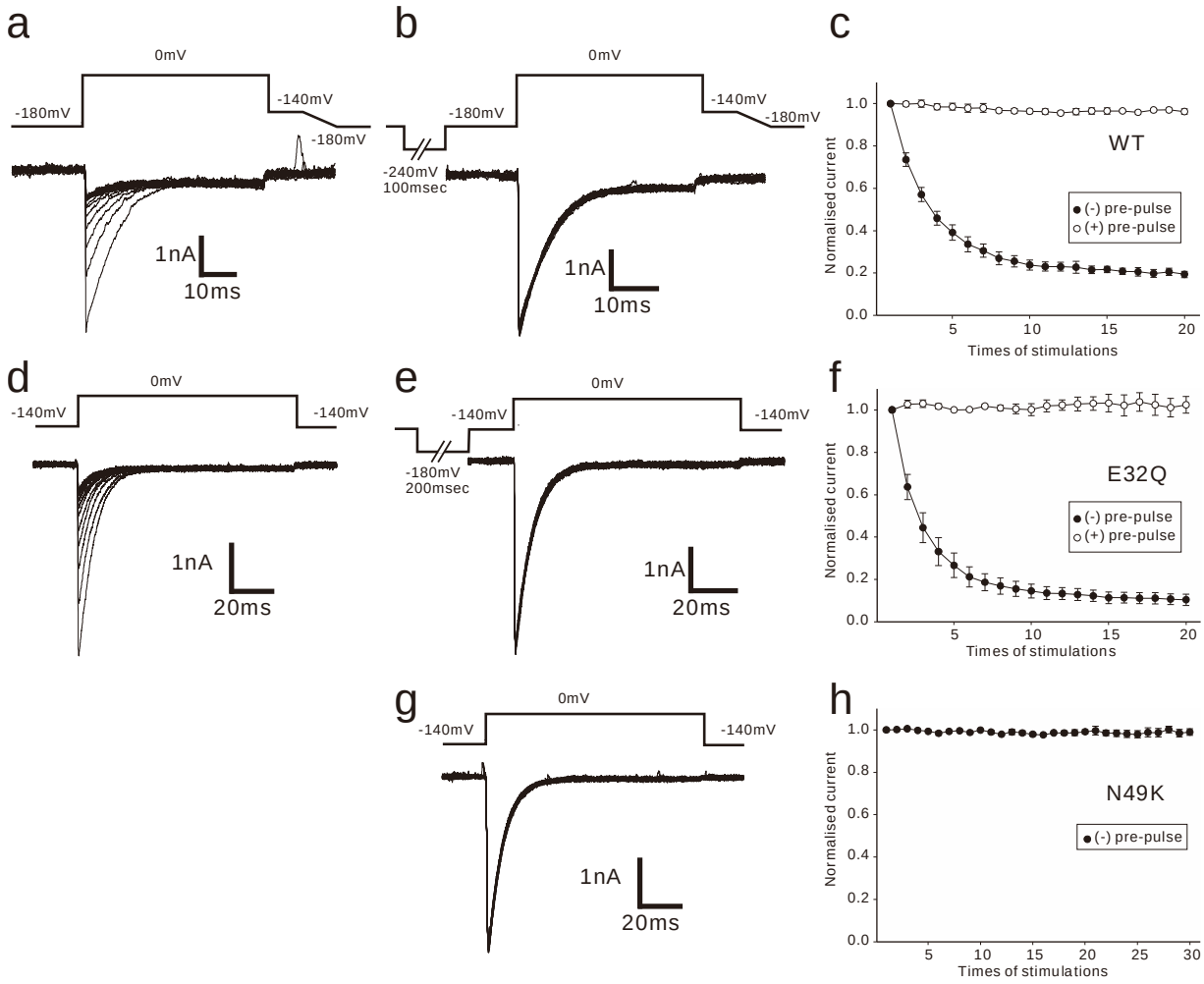
a
0mV
-180mV
-140mV
-180mV
1nA
10ms
b
0mV
-180mV
-140mV
-180mV
-240mV
100msec
1nA
10ms
c
WT
(-) pre-pulse
(+) pre-pulse
Normalised current
Times of stimulations
d
0mV
-140mV
-140mV
1nA
20ms
e
0mV
-140mV
-140mV
-180mV
200msec
1nA
20ms
f
E32Q
(-) pre-pulse
(+) pre-pulse
Normalised current
Times of stimulations
g
0mV
-140mV
-140mV
1nA
20ms
h
N49K
(-) pre-pulse
Normalised current
Times of stimulations

Figure.4

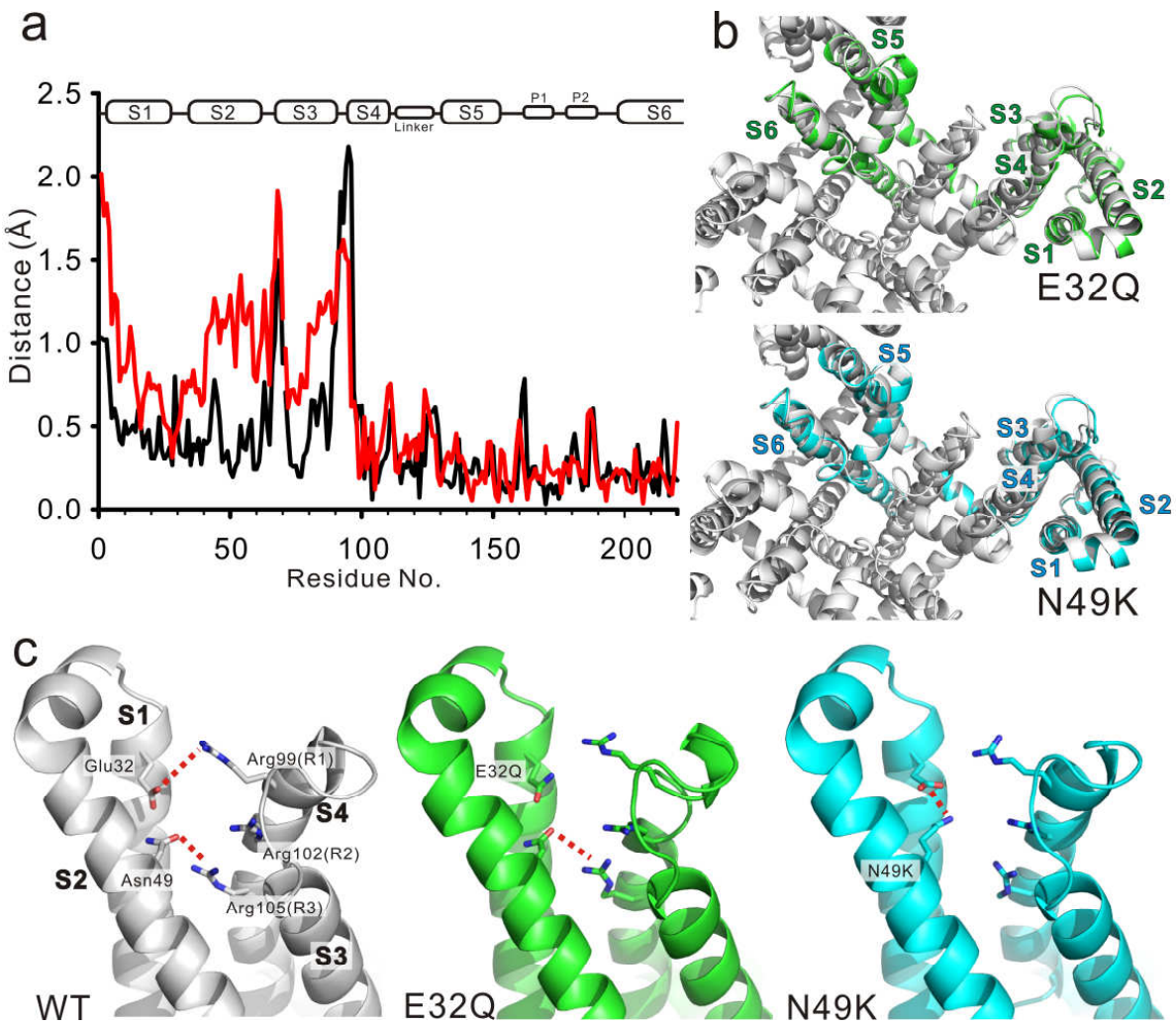
a
S1
S2
S3
S4
Linker
S5
P1
P2
S6
Distance (Å)
Residue No.
b
S5
S6
S3
S4
S2
S1
E32Q
S5
S6
S3
S4
S2
S1
N49K
c
S1
Glu32
Arg99(R1)
S4
Arg102(R2)
S2
Asn49
Arg105(R3)
S3
WT
E32Q
E32Q
N49K
N49K

Figure.5

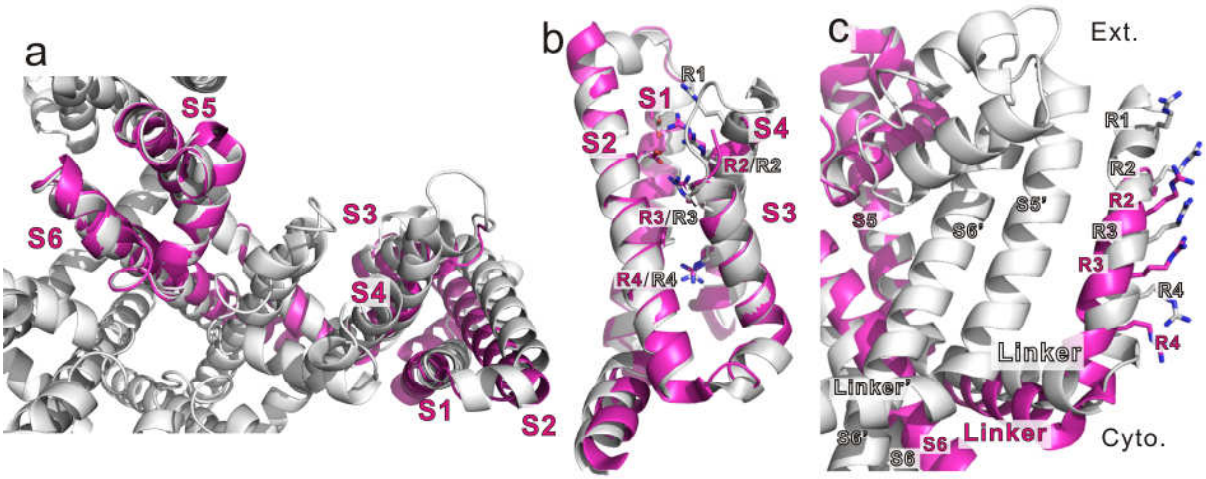
a
S5
S6
S3
S4
S1
S2
b
R1
S1
S2
S4
R2/R2
R3/R3
S3
R4/R4
c
Ext.
R1
R2
R2
S5
S6'
S5'
R3
R3
R4
R4
Linker
Linker'
S6'
S6
Linker
Cyto.

Figure.6

Supplementary Information

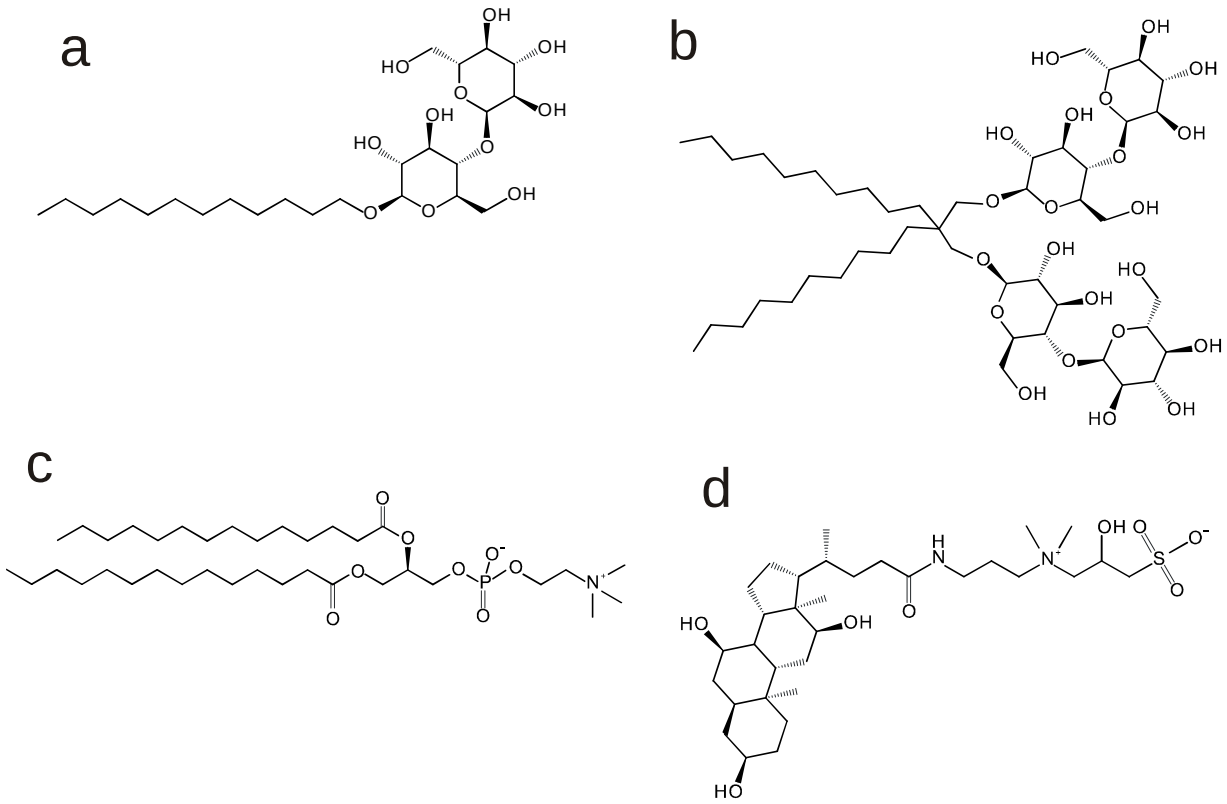

Fig. S1

Molecular formulae of detergents and lipid used in the purification and crystallization.

a, DDM (n-Dodecyl-β-D-maltoside)

b, LMNG (Lauryl maltose neopentyl glycol)

c, DMPC (1,2-Dimyristoyl-sn-glycero-3-phosphorylcholine)

d, CHAPSO (3-[(3-Cholamidopropyl)dimethylammonio]-2-hydroxypropanesulfonate)

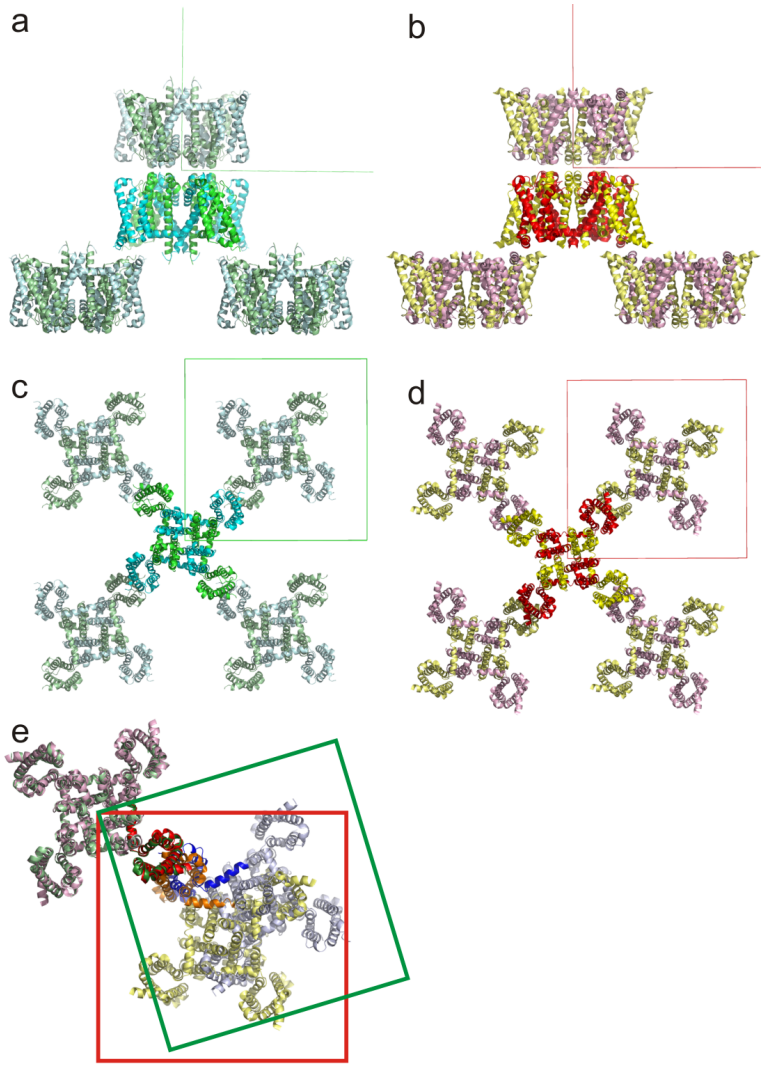

Fig. S2

Comparison of crystallographic packing of NavAb crystals in high-pH and low-pH conditions. a and b: Crystallographic packing of NavAb crystals in high-pH (a) and low-pH (b) conditions from the horizontal view, respectively. In the high-pH condition, the center molecule is colored green and cyan, and other molecules are colored pale green and pale cyan. In the low-pH condition, the center molecule is colored red and yellow, and other molecules are colored pink and pale yellow. c and d: Crystallographic packing of NavAb crystals in high-pH (c) and low-pH (d) conditions from the vertical view, respectively. e: Imposed structure of NavAb channel in the high-pH condition (pale green) on that in the low-pH condition (pink). Adjacent channel and crystal lattice are depicted as pale blue and green, and pale yellow and red in the high-pH and low-pH condition, respectively. To clarify the crystallographic packing, the VSD and S4-S5 linker concerned with adjacent channel packing are colored green and blue, and red and orange in high-pH and low-pH conditions, respectively.

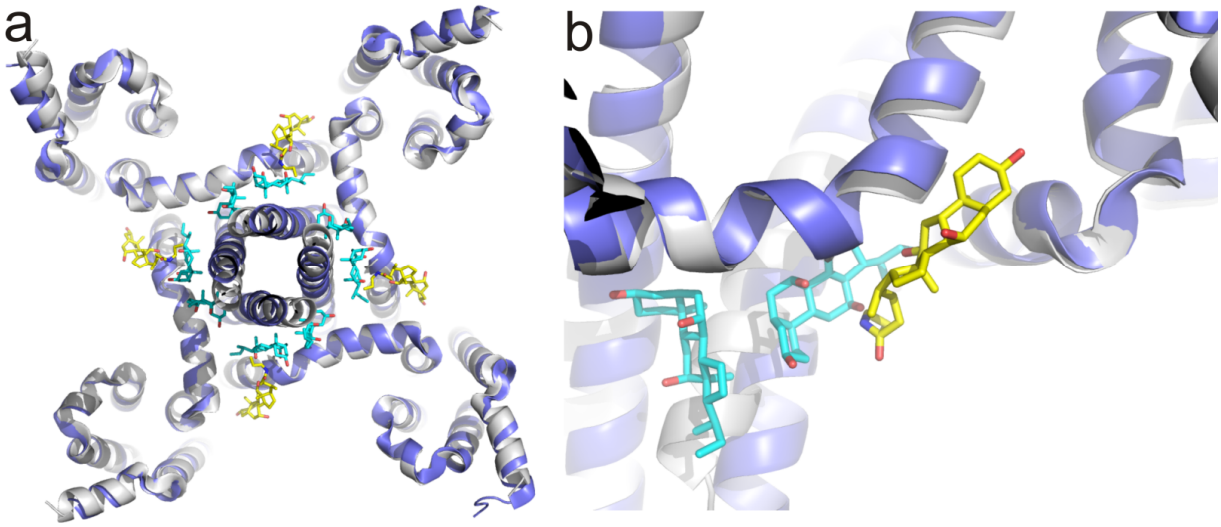

Fig. S3

Comparison of the postion of CHAPSO between the high-pH NavAb WT structure and the closed structure of NavAb mutant.

a: Structure of whole channels of closed NavAb mutant (pdb code: 5VB2) superimposed on that in a high-pH condition (white). Closed NavAb mutant is colored purple. CHAPSO observed in the high-pH NavAb WT structure and the structure of closed NavAb mutant are colored yellow and cyan, respectively. b: Focused viewing on CHAPSO position. The viewing is similar to Fig. 2f.